International Journal of Engineering

Journal Homepage: www.ije.ir

Thermal Performance of Jet Impingement with Spent Flow Management

A. Husain*, M. Ariz

Mechanical and Industrial Engineering Department, Sultan Qaboos University, Muscat, Sultanate of Oman

PAPER INFO

Paper history:
Received 20 March 2017
Received in revised form 08 May 2017
Accepted 07 July 2017

Keywords:
Jet Impingement
Effusion Holes
Spent Flow Management
Enhance Heat Transfer
Thermal Resistance
Pressure Drop

ABSTRACT

The present study proposes novel micro-jet impingement heat sink with effusion holes for flow extraction. The design consists of impingement nozzles surrounded by multiple effusion holes to take away the spent fluid. A three-dimensional numerical model is used for steady, incompressible, laminar flow and conjugate heat transfer for the performance analysis of the proposed design. The computational domain is defined by applying symmetric boundary conditions around a unit cell of the jet impingements and effusion holes. The effect of several design parameters, viz., jet diameter, effusion-hole diameter, stand-off and the jet-to-effusion pitch is investigated. A higher standoff-to-jet diameter ratio exhibited lower thermal resistance whereas lower standoff-to-jet diameter ratio exhibited lower pressure-drop. Smaller jet-to-effusion hole spacing resulted in minimum temperature-rise along with maximum total pressure-drop and heat transfer coefficients.

***doi**: 10.5829/ije.2017.30.10a.22*

1. INTRODUCTION

With the rapid advancement of electronics industries and increasing demand for high heat flux removal, the micro-cooling is gaining considerable attention from designers and researchers. Thermal designers are looking for efficient techniques of cooling and maintaining electronic components temperature at satisfactory levels to satisfy device performance and ensure its reliability. As the air cooling techniques reaching to its limits for the low-end electronics, liquid cooling provides efficient solutions for high-end electronics integration. Initially, Tuckerman and Pease [1] proposed a new method of liquid cooling in micro-channel and accomplished a removal of heat flux as much as 790 W/cm^2. Liquid flows from one end to the other end in micro-channels leaving a higher temperature at the inlet and lower temperature at the outlet [2-8] which leads to temperature non-uniformity at the substrate surface. The sensitivity, reliability, performance, and efficiency of electronic devices are highly temperature dependent and a high temperature may lead to irreparable loss of electronic product [9, 10].

*Corresponding Author's Email: *afzal19@squ.edu.om* (A. Husain)

A lot of research has been done on the macro-scale air jet impingement [11-15] and later the concept of liquid-based micro-jet was realized for electronics cooling [16-19]. Wu et al. [16] studied experimentally heat transfer characteristics of 500 μm and 550 μm single jets as well as a jet arrays with standoff (H) varying from 200 μm to 3000 μm. The study reported an area-averaged heat transfer coefficient of 320 W/m^2 K for a single jet with the diameter and standoff (H) of 500 μm and 750 μm, respectively, at the expense of 35 kPa pressure drop, and better cooling efficiency was observed at low driving pressure. Lee and Vafai [17] conducted a comparative analysis of the micro-channel and the micro-jet impingement and found that the micro-channel cooling is best-suited for heated surface smaller than 70×70 mm whereas the jet-impingement cooling offers better performance as compared to the micro-channel for a larger heated surface with proper spent flow arrangement. In order to take benefits of both the micro-channel as well as the micro-jet impingement, Sung and Mudawar [18] conducted an experimental and numerical study of a new hybrid design. They observed a decrease in temperature-rise and temperature gradients over the heated surface. For the further advancement of micro-cooling, Wang et al. [19] presented an experimental analysis of single and two-phase flow in

Please cite this article as: A. Husain, M. Ariz, Thermal Performance of Jet Impingement with Spent Flow Management, International Journal of Engineering (IJE), TRANSACTIONS A: Basics Vol. 30, No. 10, (October 2017) 1599-1608

micro-jet impingement heat sink. The jet diameter varied from 40 μm to 76 μm. The authors achieved a removal of 90 W at a flow rate of 8 ml/min with a temperature-rise of 100 ^{o}C.

The management of spent flow has been critical in jet impingement designs. The cross flow stems from impingement deteriorates the heat transfer characteristics by interfering with side jets. To counter the adverse effects of spent flow, the spent fluid is removed through effusion holes designed either at the impingement surface or at the jet plate. Significant literature is available on the former configuration in which effusion holes were made on impingement surface. Hollworth and Dagan [20] proposed a design of jet impingements along with transpiration of fluid through a vent hole on impingement surface. They found higher average heat transfer for staggered jets than the inline jets with vent holes on the impingement surface. Furthermore, they found that the arrays with staggered vent offered more heat transfer rates as compared to same arrays with edge venting. Kim et al. [21] carried out thermal stress analysis and optimization of jet impingement/effusion cooling system and observed that the cooling system of staggered jet impingement has the lowest thermal stresses when the coolant flow direction was same as the main flow. In another study, Ming et al. [22] experimentally observed that the heat transfer can be enhanced by decreasing the hole-to-hole spacing and jet-to-target spacing.

Andrews et al. [23] conducted experiments for overall heat transfer coefficient for the impingement-effusion cooling system. They used the same impingement geometry for two different holes of 2.16 mm and 3.27 mm diameter on effusion plate. The overall heat transfer was found 45% and 30% higher than the impingement heat transfer without spent flow management. Choo and Rhee [24] performed experiments for the impinging jet on effusion surface (target plate). The hole pitch-to-diameter ratio was 6.0. The gap distance between the perforated plates was ranged from 0.33 to 10 times hole diameter while the Reynolds numbers varied from 5000 to 12000. The cooling performance of staggered arrangement was found better than the shifted hole arrangement owing to strong secondary vortices. Cho et al. [25] proposed three arrangements with two perforated plates, placed one over other, in staggered, inline and in a shifted manner in one direction. They kept the thickness of effusion plate to diameter ratio and pitch to diameter ratio constant at 1.5 and 3.0, respectively, whereas the ratio of the distance between the perforated plates to hole diameters varied from 1 to 3. The overall area-averaged heat transfer for the staggered arrangement and the shifted arrangement were approximately 70–75% higher than that of the in-line arrangement for Reynolds numbers ranging from 3000 to 14000. Rhee et al. [26] proposed a new design of jet impingements on effusion surface with ribs. They investigated the effect of rib turbulators on heat transfer characteristics for the impingement-effusion cooling with initial crossflow. The rib turbulators showed better cooling performances than jet impingements without ribs.

Furthermore, few studies are available on the alternate configuration where effusion holes are designed on the jet plate. Onstad et al. [27] presented an experimental analysis of heat transfer characteristics of staggered array impingement jets of 8.46 mm diameter and jet-to-jet spacing of 2.34 times of jet diameter with spent fluid extracted through six effusion holes of 7.36 mm diameter distributed around each jet. The analysis was conducted for extraction area ratio of 2.23 and jet-to-target spacing of 1.18 times of jet diameter. The Nusselt number close to 75 was achieved at the highest Reynolds number (Re = 10000). Later, Hoberg et al. [28] studied experimentally staggered arrangement of jets with an inter-jet spacing of 2.34 times of jet diameter and observed a consistent decrease of heat transfer coefficient with the increase of standoff. In addition, smaller jets were found to be more effective in achieving high heat transfer coefficients. Smith [29] investigated three different effusion configurations with varying effusion diameters ranging from 0.5 mm to 2 mm and observed increased heat transfer coefficient for a small H/d and for an addition of ribs on the target surface. Also, pressure losses were minimum for large effective area of effusion holes. Huber and Viskanta [30] investigated the effect of spent air exit location on magnitude and uniformity of the local heat transfer coefficient of 3×3 square array.

In view of the limited literature available on micro-jet impingement with effusion scheme for liquid-based cooling methods, the present research proposes a novel jet impingement with effusion mechanism. The local heat transfer coefficient of the jet impingements decreases along the wall jet away from the stagnation zone, which can significantly be improved by suitably removing the spent flow through effusion holes. The effusion holes can be suitably arranged to facilitate removal of the spent flow. The overall performance of the model depends on several parameters, viz., jet diameter, the diameter of effusion holes, distribution of effusion holes, stand-off distance and jet pitch etc., which is inconclusive in the literature.

A three-dimensional numerical analysis was carried out through a validated numerical model to investigate thermal performance of the proposed design and to find out the effect of several design parameters on the performance.

2. DESIGN MODEL OF COUPLED JET-IMPINGEMENT-EFFUSION COOLING SYSTEM

Figure 1 shows the schematic of impingement-effusion models. The nozzles and effusion holes in the system can be designed on the back side of a copper substrate. The coolant passes through the nozzles and impinges on a heated surface where it forms stagnation zone and wall jet. While traveling away from the center fluid takes the heat and moves through the effusion holes designed on the jet plate. The dimensions of the substrate base are 20mm×20mm (Figure 1). The thickness of the substrate base (ts) and the height of the impingement channel (H) were 200 µm and 300 µm, respectively. The thickness of nozzle plate (tn) in which nozzles and effusion nozzles were designed was kept constant at 200 µm.

Computational domain defined by applying symmetric boundary conditions is shown in Figure 2(a) while Figure 2(b) shows the grid for the specified domain. For the simplified numerical model, the substrate on which these impingement nozzles and effusion holes are designed is not taken for analysis, although the nozzles, a fluid domain, and a substrate base are taken in the computational domain for analysis (Figure 2). Several geometric parameters, i.e., jet diameter (di), the diameter of effusion hole (do), stand-off (H), jet pitch (S), substrate thickness (ts), jet plate thickness (tn), affect the performance of the model.

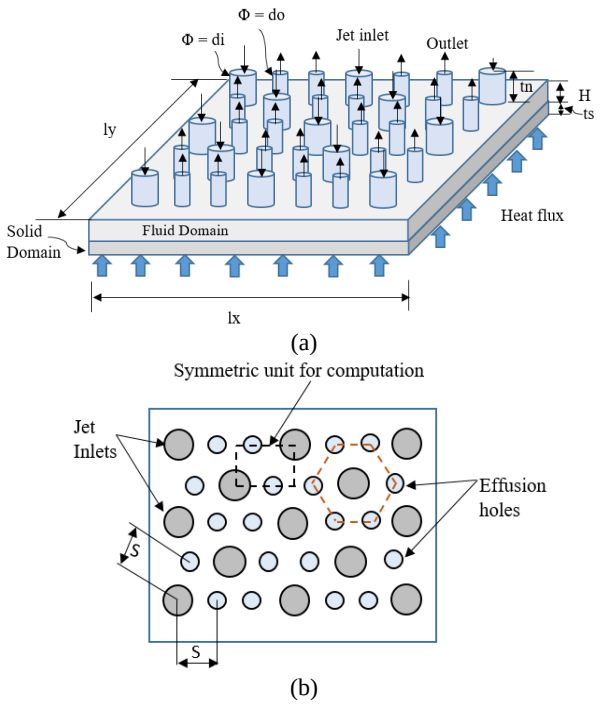

Figure 1. (a) Schematic diagram of a coupled impingement-effusion heat sink model, and (b) Cover plate

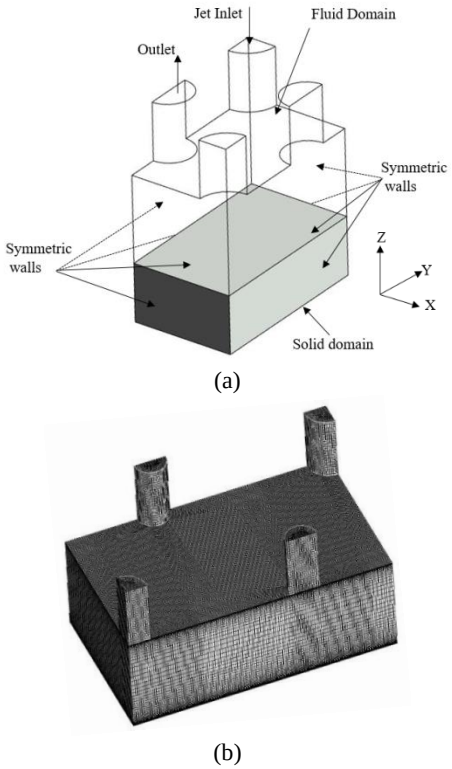

Figure 2. (a) Symmetric computational domain for a unit cell of jet impingement and effusion model, (b) grid system for unit cell

However, three design variables, viz., impingement to effusion area ratio (di^2/do^2), stand-off to jet diameter ratio (H/di), and jet pitch to diameter ratio (S/di), were selected for parametric investigation.

3. NUMERICAL ANALYSIS

The deionized ultra-filtered (DIUF) water was used as a coolant to flow through nozzles, impingement channel, and effusion holes. A constant heat flux (q = 100 W/cm^2) was applied at the base of the substrate to imitate a heat source. Three-dimensional numerical analysis of fluid flow and conjugate heat transfer was performed for the performance assessment. The mass, momentum, and energy equations which are solved for steady laminar flow are as follows [5]:

$$\nabla.(\rho_f V)=0$$

$$V.\nabla(\rho_f V)=-\nabla p+\nabla.(\mu_f \nabla V)$$

$$V.\nabla(\rho_f C_{p,f} T_f)=\nabla.(k_f \nabla T_f)$$

$$\nabla.(k_s \nabla T_s)=0$$

The above equations are solved through CFX [31] which employs the coupled algebraic multigrid method [32]. The thermo-physical properties of coolant (DIUF water) are allowed to change with temperature in an iterative procedure to take micro-scale effect into account [33, 34].

A unit symmetric cell as shown in Figures 1(b) and 2(a) is taken for computation and results were translated for the entire domain. Symmetric boundary conditions were applied at all the sides to define a computational model. The multi-block unstructured hexahedral mesh is created for the specified domain (Figure 2(b)). A constant heat flux was applied at the bottom of the heat sink. A no-slip condition was assigned at the nozzles walls, channel walls, impingement surface and the effusion holes. A constant velocity was applied at the inlet and zero relative pressure was assigned at the outlet. To reduce the computation time, the nozzle plate was not taken for computation. The nozzle walls and the fluid-domain top were kept adiabatic for conservative analysis. The flow and performance parameters are described as follows:

The Reynolds number at the jet inlet is:

$$Re = \frac{\rho V_i d_i}{\mu}$$

The overall thermal resistance is:

$$R_{th} = \frac{\Delta T_{\max}}{qL_c}$$

Here, maximum temprature-rise in the domain is:

$$\Delta T_{\max} = T_{s,\max} - T_{f,i}$$

The local heat transfer coefficient is:

$$h = \frac{k_f (\partial T / \partial \bar{n})}{(T_i - T_w)}$$

The pumping power required to drive the fluid is:

$$P = Q.\Delta p$$

Here, pressure drop is

$$\Delta p = p_{a,i} - p_{a,o}$$

4. RESULTS AND DISCUSSION

The grid dependence test is done for several performance parameters, i.e., maximum temperature-rise ($\Delta T_{\max}$), total pressure drop (Δp_t) and area-averaged heat transfer coefficient (h_{avg}). An unstructured multi-block mesh is generated to take into account higher flow gradients near the stagnation region. The grid system with nodes 360000 is found suitable for a typical design with H/d_i = 1.5 and S/d_i = 2 as shown in Figure 3.

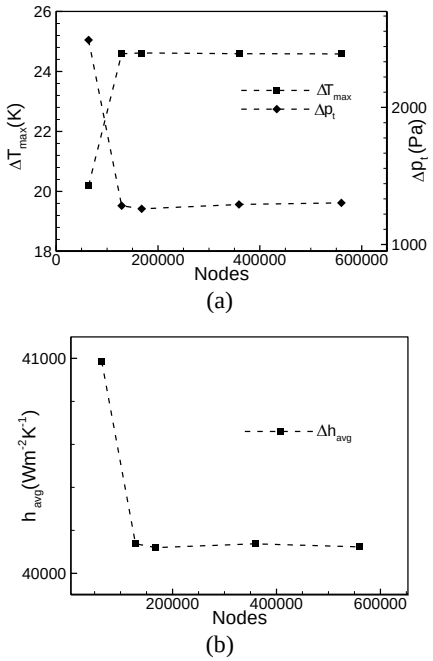

Figure 3. Grid test for (a) maximum temperature-rise ($\Delta T_{\max}$) and total pressure-drop (Δp_t) (b) area-averaged heat transfer coefficient (h_{avg})

The changes in the performance parameters are more than 2% for a change of grid from 63000 nodes to 130000 nodes, while for a change of grid from 130000 to 360000 nodes, these changes are less than 1% (Figure 3).

Any further refinement of grids produces insignificant changes in these quantities. The convergence is checked by setting the criteria for Root Mean Square (RMS) residuals below 10^{-6}. The validation of the numerical model was carried out and results were compared with that of experimental results reported by Wang et al. [19] for the maximum temperature at various levels of heat flux applied to the bottom surface. The detailed validation of the numerical model was reported in a previous study [35].

The variation of maximum temperature-rise ($\Delta T_{\max}$) of the substrate with *S*/*di* is shown in the Figure 4(a). The $\Delta T_{\max}$ increases monotonically with increasing *S*/*di* (Figure 4(a)). With the increase in *S*/*di* the pitch of jet-to-effusion hole increases which results in reduced velocity gradient in the wall jet which in turn leads to higher $\Delta T_{\max}$ at the target surface. In addition to this, a smaller jet diameter corresponding to higher *H*/*di* promotes more convective heat transfer owing to increased jet velocity, hence exhibits the lowest $\Delta T_{\max}$. The total pressure drop (Δp_t) is mainly associated with three main sections, viz. nozzles, impingement channel and effusion holes accompanied with minor losses, e.g., expansion and contraction owing to nozzles and

effusion holes, respectively. The variation in Δp_t is insignificant with increasing *S*/*di* whereas pressure drop increases with increasing *H*/*di* at constant *H*. It shows much dependence of pressure drop on the nozzle diameter (*di*).

The ΔT_{max} is found to be insensitive to any change in di^2/do^2 while Δp_t increases monotonously with an increase in di^2/do^2 due to the decrease in effusion hole diameter which consequently increases flow velocity and contributes to pressure drop (Figure 5). Also, pressure drop increases monotonously with an increase in *H*/*di*. Area-averaged heat transfer coefficient decreases monotonically with increasing *S*/*di* (Figure 6(a)). The pitch of jet-to-effusion hole increases with increasing in *S*/*di*, which leads to mitigate velocity gradients inside the jet wall.

In addition, higher jet velocity corresponding to higher *H*/*di* values causes high area-averaged heat transfer coefficient due to the thinner boundary layer. Further trade-off analysis is carried out for overall thermal resistance (R_{th}) and pumping power (*P*) as shown in Figure 6(b). These characteristics (Figure 6) provide wider perspective in the optimal paradigm with design variables. In quest of optimal design, characteristics corresponding to *S*/*di* =2.0 at *H*/*di*=1, 1.5, 2.0 show minimal overall thermal resistance with minimal pumping power. The variations of ΔT_{max} against Reynolds number (*Re*) at *H*/*di* =1 is shown in Figure 7(a).

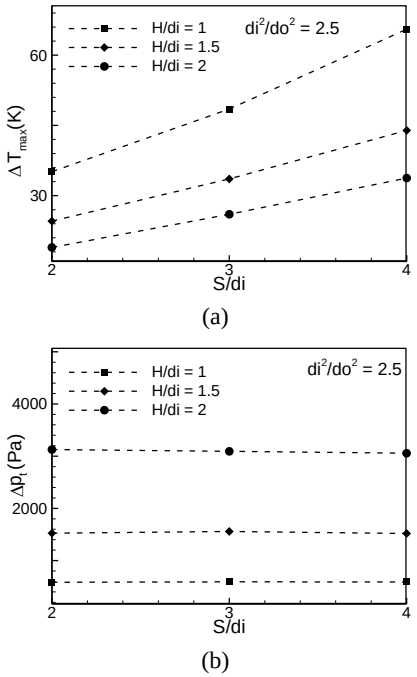

Figure 4. Variation of (a) maximum temperature-rise (ΔT_{max}) and (b) total pressure-drop (Δp_t) with S/di, for H/di =1-2, di^2/do^2 = 2.5 and Re = 200

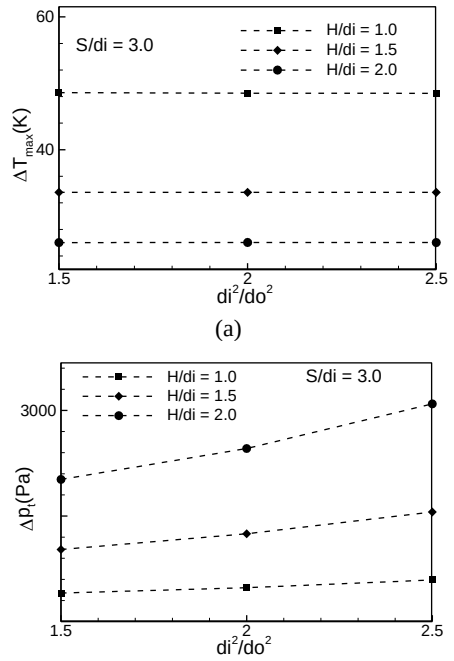

Figure 5. Variation of (a) maximum temperature-rise (ΔT_{max}) and (b) total pressure-drop (Δp_t) with di^2/do^2 for *H*/*di* =1-2 and *Re* = 200

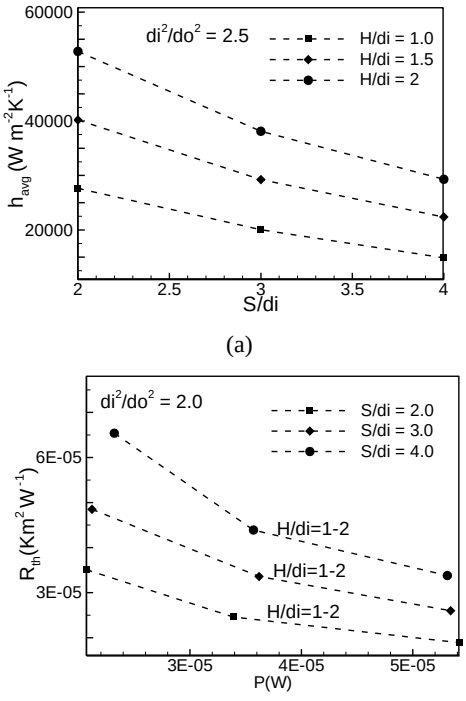

Figure 6. Variation of (a) area-averaged heat transfer coefficient (h_{avg}) with S/di and (b) functional relationship between overall thermal resistance (R_{th}) and pumping power (P) for *H*/*di* =1-2, *Re* = 200 and di^2/do^2 = 2.5

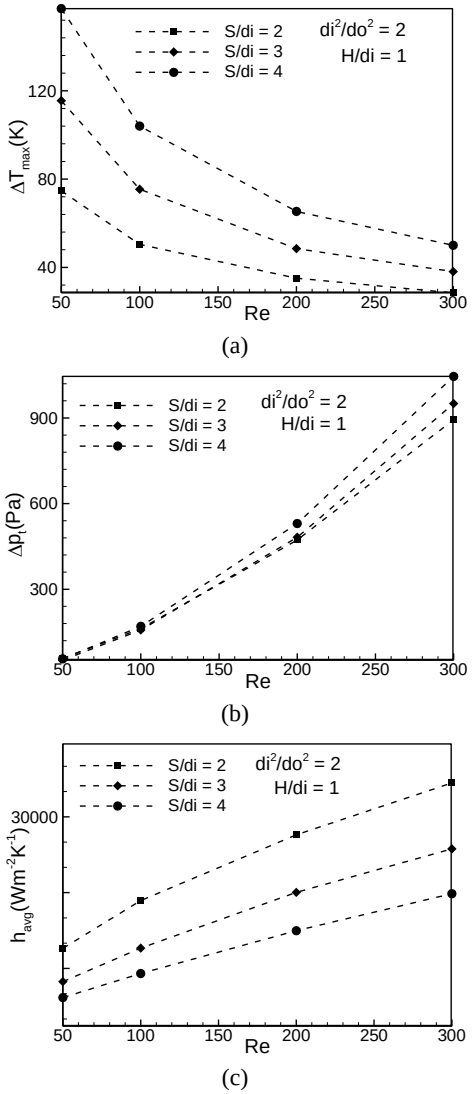

Figure 7. Variation of maximum temperature-rise (ΔT_{max}), total pressure-drop (Δp_t), and area-averaged heat transfer coefficient (h_{avg}) with Reynolds number

The trend of ΔT_{max} at substrate monotonously decreases as Reynolds number is increased. Higher jet velocity accompanied with higher Reynolds number makes the boundary layer thinner, which offers minimum thermal resistance to the heat transport.

Figure 7(b) reveals the variation of Δp_t, which occurs in nozzles, impingement channel, and effusions holes. As the Reynolds number is increased, Δp_t is increased due to higher jet velocity in nozzles. In addition to this, increased flow rate further causes a pressure-drop in impingement channel as well as in effusions holes. Figure 7(c) shows a variation of heat transfer coefficient with Reynolds numbers at *H*/*di*=1. The heat transfer coefficient which strongly depends on opon the jet velocity, increases monotonously as the jet Reynolds number increases from 50 to 300.

The temperature distribution at impingement surface reflects fluid interaction with the target surface. Figure 8 (a) shows the distribution of temperature on the impingement surface for with *S*/*di*=2-4. Temperature increases at impingement surface with decreasing uniformity as *S*/*di* increases due to increased thickness of boundary layer before the spent flow leaves through effusion holes. At *S*/*di* = 2, impingement zone at target surface is not distinguishable while for *S*/*di* = 3, 4, stagnation zone are clearly visible.

Further, Figure 8(b) shows temperature distribution with *H*/*di* = 1-2. With increasing *H*/*di*, impingement velocity increases which results in temperature decrease at impingement surface. Further temperature distribution with varying di^2/do^2 = 1.5-2.5 is shown in Figure 8(c). The temperature distribution is almost similar for all di^2/do^2 ratios. The low-temperature zone occurs at the impingement point and the temperature gradually increases as the fluid moves radially away from the stagnation point. In addition to this, high-temperature spots are seen at the impingement surface below the effusion holes.

Figure 9(a) shows the distribution of local heat transfer coefficient on impingement surface for *S*/*di*=2, 3, 4.

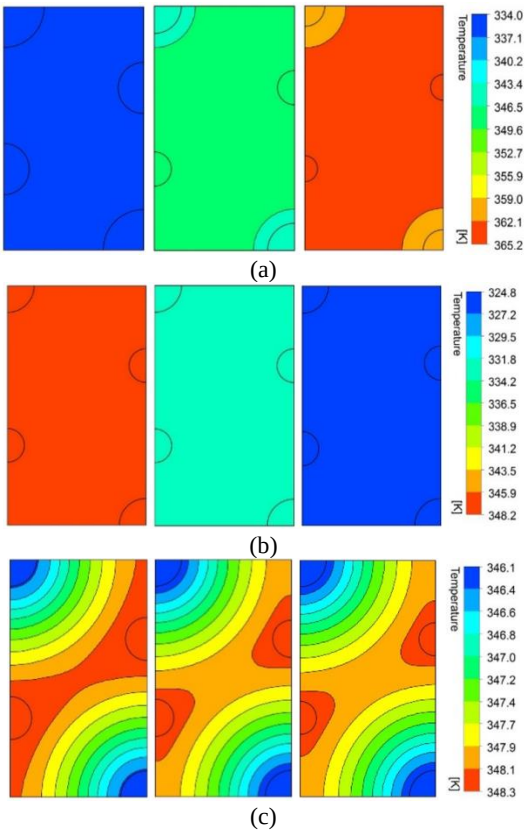

Figue 8. Temperature distribution on impingement surface with (a) *S*/*di*=2-4 at *H*/*di*=1.0, di^2/do^2=2.5 (b) *H*/*di*=1-2 at *S*/*di*=3.0, di^2/do^2=2.5 and (c) di^2/do^2=1.5-2.5 at *S*/*di*=3.0, *H*/*di*=1

The local heat transfer coefficient is higher at the impingement point and it is gradually decreasing as the fluid moves away from the stagnation point, and low heat transfer zone is established near the effusion holes.

Moreover, heat transfer coefficient increases at the impingement point with increasing H/di from 1 to 2, owing to lower resistance to heat flux (Figure 9(b)). Similar heat transport patterns are obtained with a change of di^2/do^2 from 1.5 to 2.5 (Figure 9(c)).

A comparative analysis is done for the proposed design (Design-1) with other two designs (Design-2 and Design-3) for different performance parameters, viz., maximum temperature-rise (ΔT_{max}), total pressure drop (Δp_t), and area-averaged heat transfer coefficient (h_{avg}). The jet plate with the three designs, i.e., proposed jet impingement effusion design (Design-1), Design-2 ([28]) and a basic jet-impingements with effusion-holes design (Design-3) is shown in Figure 10. In Design-1 and Design-2, the effusion holes are distributed around the impinging jet in a hexagonal manner but the proposed design (Design-1) shows a uniform distribution of jets and effusion holes as compared to Design-2 [28]. Figure 11(a) shows the maximum temperature-rise with Reynolds number (Re = 50-300) for all the three designs.

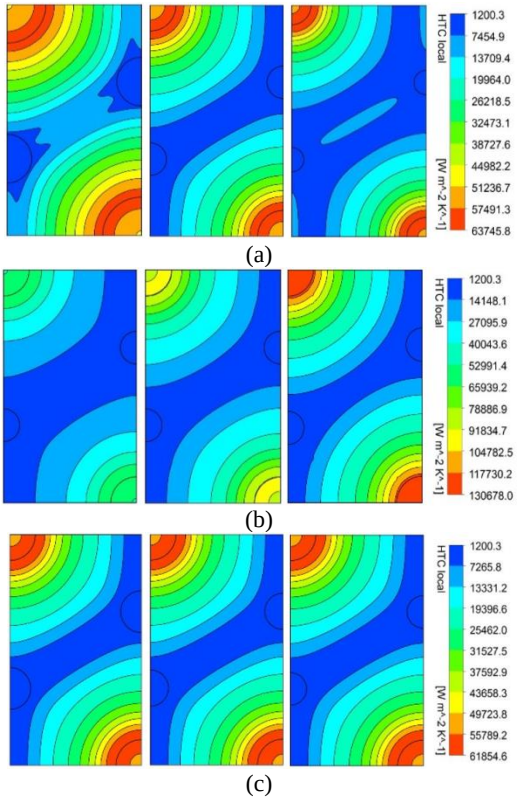

Figure 9. Local heat transfer coefficient on impingement surface with (a) S/di=2-4 at H/di=1.0, di^2/do^2=2.5 (b) H/di=1-2 at S/di=3.0, di^2/do^2=2.5 and (c) di^2/do^2 =1.5-2.5 at S/di=3.0, H/di=1

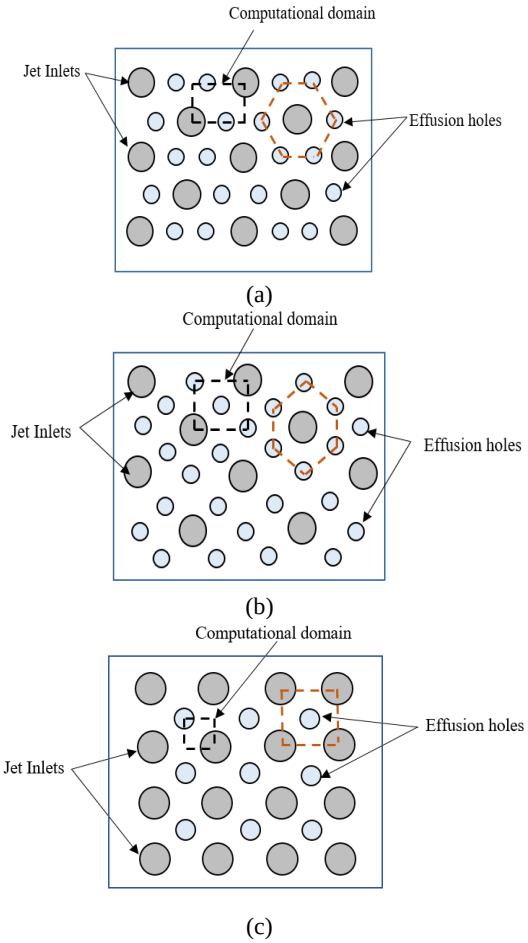

Figure 10. Jet plate models for (a) Design-1, (b) Design-2 [28] and (c) Design-3

The temperature-rise of the proposed design is closely matched with the Design-2, which reveals that heat transfer coefficient is less sensitive to the arrangement of effusions holes around the jet nozzle. Further, Design-3 shows large temperature-rise as compared to the other two designs.

Figure 11(b) shows the variation of total pressure drop with Reynolds number (Re = 50-300). The Δp_t increases monotonously with Reynolds number for all the three designs. Design-2 offers less pressure drop than the other two designs. Area-averaged heat transfer coefficient, which reflects jet impingement effectiveness in the model is compared for the three designs (Figure 11(c)). Increases in Reynolds number results in an increase of area-averaged heat transfer coefficient (Figure 11(c)). Higher heat transfer rate is achieved for thinner stagnation zone, which is associated with the higher Reynolds number. Heat transfer characteristics of Design-1 overlaps to Design-2 while Design-3 deviates from Design-1 and Design-2 at higher Reynolds number with lower values of heat transfer coefficient.

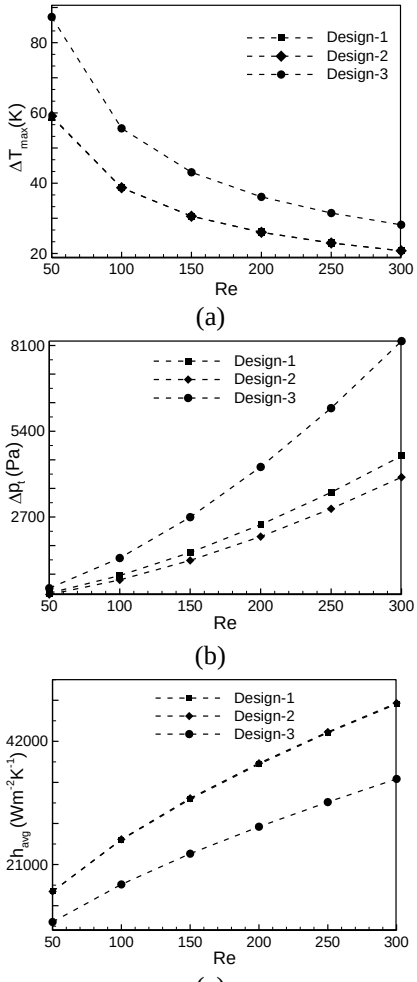

Figure 11. Variation of (a) maximum temperature-rise (ΔT_{max}), (b) total pressure-drop (Δp_t) (c) area-averaged heat transfer coefficient (h_{avg}) with Reynolds number (Re) = 50-300 for Design-1, Design-2 and Design-3

Figure 12 compares the temperature contours of the proposed design with Design-2 and Design-3. Temperature distribution for the proposed design is similar to that of the Design-2 having distinguishable impingement zones, unlike Design-3. In addition to this, Design-3 has more impingement temperature than the other two design. All the three designs show a similar distribution of heat transfer coefficient with stagnation and effusion zones. The proposed design shows almost similar heat transfer coefficient patterns as the Design-2, whereas, in the case of Design-3, a larger stagnation zone is appeared along with a larger effusion zone.

6. CONCLUDING REMARKS

This study proposes a novel micro-jet impingement heat sink model with spent flow management through effusion holes.

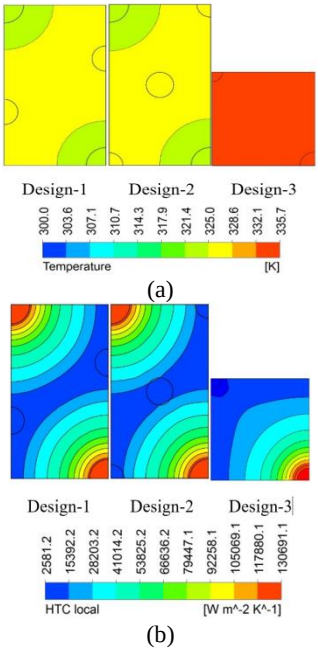

Figure 12. (a) Temperature distribution and (b) local heat transfer coefficient at impingement surface for Design-1 Design-2 and Design-3

A three-dimensional numerical analysis was carried out to understand the effect of design parameters, viz., ratios of the pitch-to-jet diameter, stand off-to-jet-diameter and area ratio of jet-to-effusion holes on the performance parameters, viz., maximum temperature-rise, total pressure-drop, area-averaged heat transfer coefficient, overall thermal resistance and pumping power.

The smaller jets and smaller jet-to-effusion holes spacing results in higher heat transfer coefficient, lower temperature-rise but higher pressure-drop. The pressure-drop shows small sensitivity to jet-to-effusion spacing, although, it is largely dependent upon nozzle and effusion holes. The temperature-rise decreases while pressure-drop and heat transfer coefficient increase consistently with Reynolds number. Lower pumping power and thermal resistance are associated with lower jet-to-effusion hole spacing. Lower temperature and higher heat transfer coefficient zones are located around the impingement and higher temperature and lower heat transfer coefficients are located around the effusion holes.

7. ACKNOWLEDGEMENTS

Authors acknowledge the support of Sultan Qaboos University through Internal Research Grant (IG/ENG/MEID/14/03) and Collaborative Research Grant (CL/SQU-UAEU/15/02) for conducting this research.

8. REFERENCES

1. Tuckerman, D.B. and Pease, R., "High-performance heat sinking for vlsi", ***IEEE Electron Device Letters***, Vol. 2, No. 5, (1981), 126-129.
2. Kawano, K., Sekimura, M., Minakami, K., Iwasaki, H. and Ishizuka, M., "Development of micro channel heat exchanging", ***JSME International Journal Series B Fluids and Thermal Engineering***, Vol. 44, No. 4, (2001), 592-598.
3. Qu, W. and Mudawar, I., "Experimental and numerical study of pressure drop and heat transfer in a single-phase micro-channel heat sink", ***International Journal of Heat and Mass Transfer***, Vol. 45, No. 12, (2002), 2549-2565.
4. Toh, K., Chen, X. and Chai, J., "Numerical computation of fluid flow and heat transfer in microchannels", ***International Journal of Heat and Mass Transfer***, Vol. 45, No. 26, (2002), 5133-5141.
5. Liu, D. and Garimella, S.V., "Analysis and optimization of the thermal performance of microchannel heat sinks", in ASME International Electronic Packaging Technical Conference and Exhibition, American Society of Mechanical Engineers. (2003), 557-565.
6. Husain, A. and Kim, K.-Y., "Microchannel heat sink with designed roughness: Analysis and optimization", ***Journal of Thermophysics and Heat Transfer***, Vol. 22, No. 3, (2008), 342-351.
7. Husain, A. and Kim, K.-Y" ,.Optimization of a microchannel heat sink with temperature dependent fluid properties", ***Applied Thermal Engineering***, Vol. 28, No. 8, (2008), 1101-1107.
8. Khameneh, P.M., Mirzaie, I., Pourmahmoud, N., Rahimi, M. and Majidyfar, S., "A numerical study of single-phase forced convective heat transfer in tube in tube heat exchangers", ***World Academy of Science, Engineering and Technology, International Journal of Mechanical, Aerospace, Industrial, Mechatronic and Manufacturing Engineering***, Vol. 4, No. 10, (2010), 958-963.
9. Hamann, H.F., Weger, A., Lacey, J.A., Hu, Z., Bose, P., Cohen, E. and Wakil, J., "Hotspot-limited microprocessors: Direct temperature and power distribution measurements", ***IEEE Journal of Solid-State Circuits***, Vol. 42, No. 1, (2007), 56-65.
10. Dhass, A., Natarajan, E. and Lakshmi, P., "An investigation of temperature effects on solar photovoltaic cells and modules", ***International Journal of Engineering***, Vol. 27, (2014), 136-142.
11. Martin, H., "Heat and mass transfer between impinging gas jets and solid surfaces", ***Advances in Heat Transfer***, Vol. 13, (1977), 1-60.
12. Jambunathan, K., Lai, E., Moss, M. and Button, B., "A review of heat transfer data for single circular jet impingement", ***International journal of heat and fluid flow***, Vol. 13, No. 2, (1992), 106-115.
13. Webb, B. and Ma, C.-F., "Single-phase liquid jet impingement heat transfer", ***Advances in heat transfer***, Vol. 26, No., (1995), 105-217.
14. Womac, D., Incropera, F. and Ramadhyani, S., "Correlating equations for impingement cooling of small heat sources with multiple circular liquid jets", ***ASME Transactions Journal of Heat Transfer***, Vol. 116, (1994), 482-486.
15. Garimella, S.V. and Rice, R., "Confined and submerged liquid jet impingement heat transfer", ***Transactions-American Society of Mechanical Engineers Journal of Heat Transfer***, Vol. 117, (1995), 871-877.
16. Wu, S., Mai, J., Tai, Y. and Ho, C., "Micro heat exchanger by using mems impinging jets", in Micro Electro Mechanical Systems,. MEMS'99. Twelfth IEEE International Conference on, IEEE., (1999), 171-176.
17. Lee, D.-Y. and Vafai, K., "Comparative analysis of jet impingement and microchannel cooling for high heat flux applications", ***International Journal of Heat and Mass Transfer*** ,Vol. 42, No. 9, (1999), 1555-1568.
18. Sung, M.K. and Mudawar, I., "Effects of jet pattern on single-phase cooling performance of hybrid micro-channel/micro-circular-jet-impingement thermal management scheme", ***International Journal of Heat and Mass Transfer***, Vol. 51, No. 19, (2008), 4614-4627.
19. Wang, E.N., Zhang, L., Jiang, L., Koo, J.-M., Maveety, J.G., Sanchez, E.A., Goodson, K.E. and Kenny, T.W., "Micromachined jets for liquid impingement cooling of VLSI chips", ***Journal of Microelectromechanical Systems***, Vol. 13, No. 5, (2004), 833-842.
20. Hollworth, B., Lehmann, G. and Rosiczkowski, J., "Arrays of impinging jets with spent fluid removal through vent holes on the target surface, part 2: Local heat transfer", ***Journal of Engineering for Power***, Vol. 105, No. 2, (1983), 393-402.
21. Kim, K.M., Moon, H., Park, J.S. and Cho, H.H., "Optimal design of impinging jets in an impingement/effusion cooling system", ***Energy***, Vol. 66, (2014), 839-848.
22. Xiao-ming, T., Jing-zhou, Z. and Hua-sheng, X" ,.Experimental investigation on impingement/effusion cooling with short normal injection holes", ***International Communications in Heat and Mass Transfer***, Vol. 69, (2015), 1-10.
23. Andrews, G., Asere, A., Hussain, C., Mkpadi, M. and Nazari, A., "Impingement/effusion cooling: Overall wall heat transfer", ***ASME paper***, No. 88-GT, (1988), 290-299.
24. Cho, H.H. and Rhee, D.H., "Local heat/mass transfer measurement on the effusion plate in impingment/effusion cooling system", in ASME Turbo Expo 2000: Power for Land, Sea, and Air, American Society of Mechanical Engineers., (2000), V003T001A058-V003T001A058.
25. Cho, H.H., Rhee, D.H. and Goldstein, R., "Effects of hole arrangements on local heat/mass transfer for impingement/effusion cooling with small hole spacing", ***Journal of Turbomachinery***, Vol. 130, No. 4, (2008), 041003.
26. Rhee, D.H., Choi, J.H. and Cho, H.H., "Flow and heat (mass) transfer characteristics in an impingement/effusion cooling system with crossflow", in ASME Turbo Expo :Power for Land, Sea, and Air, American Society of Mechanical Engineers., (2002), 865-875.
27. Onstad, A.J., Elkins, C.J., Moffat, R.J. and Eaton, J.K., "Full-field flow measurements and heat transfer of a compact jet impingement array with local extraction of spent fluid", ***Journal of Heat Transfer***, Vol. 131, No. 8, (2009), 082201.
28. Hoberg, T.B., Onstad, A.J. and Eaton, J.K., "Heat transfer measurements for jet impingement arrays with local extraction", ***International Journal of Heat and Fluid Flow***, Vol. 31, No. 3, (2010), 460-467.
29. Smith, B., "Simulation of heat/mass transfer of a three-layer impingement/effusion cooling system", (2012).
30. Huber, A. and Viskanta, R., "Convective heat transfer to a confined impinging array of air jets with spent air exits", ***Journal of Heat Transfer***, Vol. 116, No. 3, (1994), 570-576.
31. CFX-Solver, A., "Theory guide", ***Release ll***, Vol., No., (2006.(
32. Raw, M., "Robustness of coupled algebraic multigrid for the navier-stokes equations", ***AIAA paper***, Vol. 96, (1996), 0297-305.
33. Bergman, T.L. and Incropera, F.P., "Fundamentals of heat and mass transfer, John Wiley & Sons, (2011).

34. Ramiar, A. and Ranjbar, A.A., "Effects of viscous discipation and variable properties on nanofluids flow in two dimensional microchannels", ***International Journal of Engineering, Transactions A: Basics***, Vol. 24, No. 2, (2011), 131-142.

35. Husain, A., Ariz, M., Al-Rawahi, N.Z. and Ansari, M.Z., "Thermal performance analysis of a hybrid micro-channel,-pillar and-jet impingement heat sink", ***Applied thermal engineering***, Vol. 102, (2016), 989-1000.

Thermal Performance of Jet Impingement with Spent Flow Management

A. Husain, M. Ariz

Mechanical and Industrial Engineering Department, Sultan Qaboos University, Muscat, Sultanate of Oman

P A P E R I N F O

Paper history:
Received 20 March 2017
Received in revised form 08 May 2017
Accepted 07 July 2017

Keywords:
Jet Impingement
Effusion Holes
Spent Flow Management
Enhance Heat Transfer
Thermal Resistance
Pressure Drop

چکیده

تحقیق حاضر، مبدل حرارتی مجهز به میکرو جت با حفره های افیوژن را برای استخراج جریان پیشنهاد می کند. این طراحی شامل نازل های ضربه ای محاصره شده توسط سوراخ های متعدد عایق است تا مایع منتقل شده را از بین ببرد. یک مدل عددی سه بعدی برای جریان پایدار، غیر متراکم، جریان انعطاف پذیر و انتقال حرارت متناوب برای تحلیل عملکرد طراحی پیشنهادی استفاده می شود. دامنه محاسباتی با استفاده از شرایط مرزی متقارن در اطراف یک سلول واحد جابجایی جت و سوراخ افقی است. اثر تعدادی از پارامترهای طراحی، به عنوان مثال، قطر جت، قطر افقی دیافراگم، stand-off و درجه جت به افیوژن بررسی شده است. نسبت بالاتر قطر جت به stand-off، مقاومت حرارتی پایین تر را نشان می دهد، در حالی که نسبت کمتر قطر standoff به جت نشان دهنده افت فشار پایین تر است. فاصله کمتر دیافراگم جت به افیوژن منجر به حداقل افزایش درجه حرارت همراه با حداکثر افت فشار کل و ضریب انتقال حرارت شد.

***doi**: 10.5829/ije.2017.30.10a.22*